ORIGINAL ARTICLE

Multiomic, Histologic, and scRNA-seq Profiling of Pleural Mesothelioma Reveals Negative Prognosis Associated With a Novel Uncommitted Molecular Phenotype

David T. Severson, MD, DPhil,[a,b] Samuel Freyaldenhoven, MD,[a] Benjamin Wadowski, MD,[a] Yin P. Hung, MD, PhD,[c] Travis Hughes, MD, PhD,[d,e,f] Beow Y. Yeap, PhD,[g] William G. Richards, PhD,[a] Sanna Laaksonen, MD, PhD,[h] Lucian Chirieac, MD,[h] Matthew B. Couger, PhD,[a] Roderick V. Jensen, PhD,[a] Ahmed A. Sadek, MD,[a] Ilkka Ilonen, MD, PhD,[a] Kimberly Vermilya, MD,[a] Simona Innocenti, BS,[a] Stephanie L. Korle, PhD,[a] Julianne S. Barlow, MS, MCPHS,[a] Jamie Anderson, MS,[a] Jason Meyerovitz, BS,[a] Vivian Wang, MD,[a] Mary N. Dao, MS,[a] Alex K. Shalek, PhD,[d,e,f] Assunta De Rienzo, PhD,[a] Raphael Bueno, MD[a,*]

[a]*The Thoracic Surgery Oncology Laboratory and the International Mesothelioma Program (www.impmeso.org), Division of Thoracic Surgery and the Lung Center, Brigham and Women's Hospital, and Harvard Medical School, Boston, Massachusetts*
[b]*Duke University Health System, Durham, North Carolina*
[c]*Department of Pathology, Massachusetts General Hospital and Harvard Medical School, Boston, Massachusetts*
[d]*Ragon Institute of MGH, Harvard, and MIT, Cambridge, Massachusetts*
[e]*Department of Chemistry, Institute for Medical Engineering and Sciences (IMES) and Koch Institute for Integrative Cancer Research, MIT, Cambridge, Massachusetts*
[f]*Broad Institute of MIT and Harvard, Cambridge, Massachusetts*
[g]*Department of Medicine, Massachusetts General Hospital and Harvard Medical School, Boston, Massachusetts*
[h]*Department of Pathology, Brigham and Women's Hospital and Harvard Medical School, Boston, Massachusetts*

Received 27 August 2025; revised 13 November 2025; accepted 22 November 2025
Available online - 28 November 2025

ABSTRACT

Introduction: Multiomics pleural mesothelioma (PM) studies have identified prognostic molecular subsets of PM histologic types, epithelioid (ePM), biphasic (bPM), and sarcomatoid (sPM), defined by relative tumor cell content. However, the underlying biology modulating survival remains unknown.

Methods: Using 93 samples from 40 patients, we performed single-cell RNA sequencing (scRNA-seq), bulk exome and RNA sequencing, optical genome mapping, spatial transcriptomics, and histologic analyses to identify candidate drivers and prognostic biomarkers of malignant cell (MC) state.

Results: We identified a novel uncommitted MC state enriched in bPM tumors. Using inferred copy number variants, we observed all three MC states within individual clones suggesting MC state is not clonally restricted. We identified TGF-β and GAS6-AXL signaling as candidate MC state drivers for further study. Finally, we validated two prognostic MC state immunohistochemistry biomarkers, MEST (uncommitted) and MSLN (epithelioid).

Conclusions: These multiomic, scRNA-seq analyses of primary patient tissues provide new candidate drivers of MC state and novel biomarkers to improve patient stratification. Further experimental exploration and clinical validation of these findings may reveal new treatment strategies and refine current clinical decision-making in PM.

***Corresponding author.**

Drs. Severson and Freyaldenhoven contributed equally to this work.

Address for correspondence: Raphael Bueno, MD, Division of Thoracic Surgery, Brigham and Women's Hospital, 75 Francis Street, Boston, MA 02115. E-mail: rbueno@bwh.harvard.edu

Cite this article as: Severson DT, Freyaldenhoven S, Wadowski B, et al. Multiomics, histologic, and scRNA-seq profiling of pleural mesothelioma reveals negative prognosis associated with a novel uncommitted molecular phenotype. *J Thorac Oncol* 2026;21:103529

© 2025 The Authors. Published by Elsevier Inc. on behalf of International Association for the Study of Lung Cancer. This is an open access article under the CC BY-NC-ND license (http://creativecommons.org/licenses/by-nc-nd/4.0/).

ISSN: 1556-0864

https://doi.org/10.1016/j.jtho.2025.11.019

© 2025 The Authors. Published by Elsevier Inc. on behalf of International Association for the Study of Lung Cancer. This is an open access article under the CC BY-NC-ND license (http://creativecommons.org/licenses/by-nc-nd/4.0/).

Keywords: Pleural mesothelioma; Tumor micro-environment; Single cell RNA-seq; Cancer cell heterogeneity; Mesothelioma prognosis; Spatial transcriptomics

Introduction

Pleural mesothelioma (PM) is a rare, lethal cancer associated with asbestos exposure.[1–4] Three histotypes are recognized—epithelioid (ePM), biphasic (bPM), and sarcomatoid (sPM)—which are prognostic[5] and predictive (immunotherapy benefit greatest in non-epithelioid tumors[6,7]). Histotypes indicate relative morphologic epithelioid and sarcomatoid proportions: ePM if more than 90% epithelioid MCs, sPM if more than 90% sarcomatoid MCs, and bPM otherwise. Bulk RNA sequencing (RNA-seq) of tumor samples identified epithelial-mesenchymal transition (EMT) and inflammation as major axes of PM molecular variation.[8–14] Therapeutic options remain limited[4] due to lack of targetable oncogenes, within-patient, and tumor microenvironment (TME) heterogeneity.[15] Because bulk molecular studies cannot parse malignant cell (MC) versus TME features, the effects of genetic, TME, or MC characteristics on histopathologic state, stroma, and immune TME remain unknown. Recent single-cell RNA-seq (scRNA-seq) analysis of 13 patients provided the first MC variation and TME catalog in PM and identified programs associated with poor prognosis.[16]

We expand on existing scRNA-seq PM data, combining scRNA-seq of 93 anatomically mapped surgical samples from 40 patients with histopathology, adjacent bulk RNA-seq, spatial transcriptomics, and DNA optical genome mapping (OGM) of copy number variants (CNVs). We demonstrate that epithelial-mesenchymal (EM) gradient is a property of MCs and describe a novel MC-specific EM gene program (termed uncommitted) with low expression of both sarcomatoid and epithelioid programs. We use OGM and inferred scRNA-seq variants to demonstrate that MC state is not clonal and identify candidate EMT drivers within the TME including GAS6-AXL signaling. Finally, we propose immunohistochemistry (IHC) classification tests that can stratify patients for clinical decision making using newly identified biomarkers for epithelioid and uncommitted MC states.

Materials and Methods

A multimodal analytic strategy was used across PM resections, integrating single-cell transcriptomics, bulk and spatial profiling, tissue microarrays, and survival analyses. Complete, detailed protocols are provided in the Supplementary Methods.

Sample Collection and Experimental Design

Patients undergoing radical pleurectomy at Brigham and Women's Hospital (2015–2025) were enrolled under Dana-Farber Cancer Institute IRB protocol #98-063. Written informed consent permitted tissue banking, molecular analysis, and data publication. At surgery, systematic multisite pleural sampling was performed, and fresh or frozen tissue was allocated to scRNA-seq, bulk RNA-seq, exome sequencing, OGM, and histopathology. Tumor cellularity and histology were confirmed by pathologists.

scRNA-seq Data Collection and Analysis

Fresh tumors were dissociated into single-cell suspensions and processed using the Seq-Well platform. Reads were aligned to hg38 with STAR and quantified with DropSeq tools. Cells were filtered using quality metrics including detected UMIs, expressed genes, and mitochondrial expression fraction. Normalization and clustering were performed with SCTransform and Seurat. MCs were identified using CNV inference, clonotype distribution, and entropy-based clustering. Subclonal analysis was performed with inferCNV. Malignant programs (epithelioid, sarcomatoid, uncommitted) were defined using the first principal component, which correlated with published PM epithelial-mesenchymal scores.

Additional Tissue Analyses

Bulk RNA-seq was performed on 89 samples and processed with STAR and edgeR. Whole-exome sequencing identified somatic single-nucleotide variants (SNVs), CNVs, and loss of heterozygosity, whereas OGM provided genome-wide CNV detection. Spatial transcriptomics (10× Xenium in situ) and spatial proteomics (Akoya PhenoCycler) further profiled MC state in tissue context. Histopathology assessed histology, cellular composition, and inflammation across adjacent tissue samples.

Tissue Microarray Analysis

Four TMAs were constructed from 452 PMs. Multiple 1.0 mm cores were stained for MSLN and MEST. Immunohistochemistry was scored using H-score (0–300), taking mean observed across replicates.

Statistical Analysis

Differential expression was tested with Wilcoxon ranked sum comparisons. Gene set enrichment analysis (GSEA) was performed on canonical and disease-specific signatures. Expression signatures were scored and

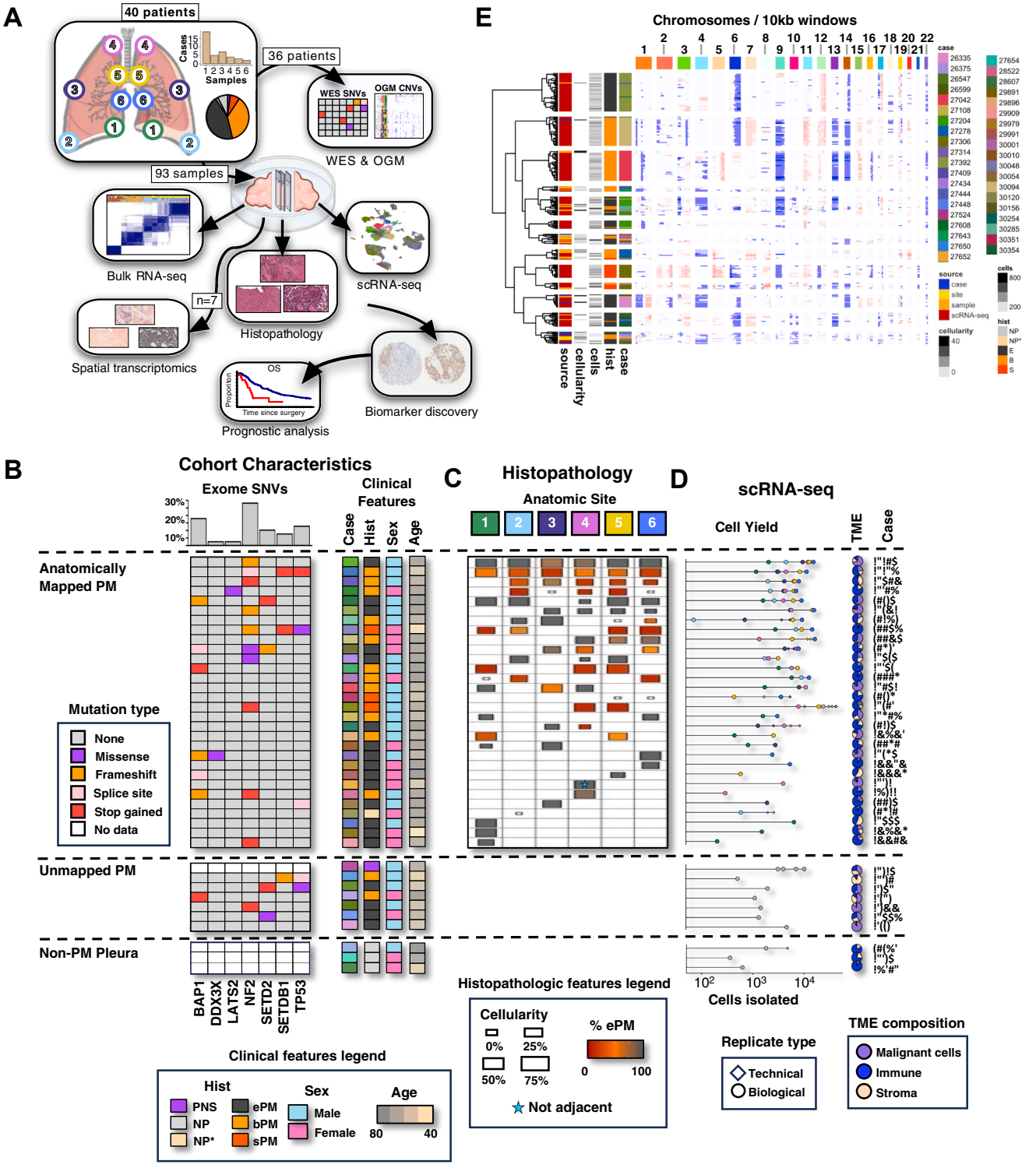

Figure 1. Comprehensive profiling of PM using scRNA-seq and multisite sampling. (*A*) Schematic illustrates experimental design and visual abstract for characterizing genomic profile of 40 patients and tumor microenvironment across multiple sites (>5 cm apart) using bulk RNA-seq, scRNA-seq, and histopathology for 93 samples. The distribution of samples collected per case and the cohort histology are also displayed, where site numbers indicate anatomic mapping with associated color scheme. (*B*) Somatic mutations in known PM driver genes are displayed in heatmap. Histology (ePM, epithelioid; bPM, biphasic; sPM, sarcomatoid; PNS, peripheral nerve sheath tumor; NP, non-PM pleura; NP*, no MCs on adjacent slide), sex, and age are annotated by color. Each row represents a separate patient resection each annotated with a unique color. The barplot above summarizes the genetic perturbations to frequently mutated genes within the cohort and the line plot to the right displays the total SNV and CNV burden of samples. (*C*) Histopathologic analysis of samples for each case is displayed

compared across MC states and TME categories using Wilcoxon ranked sum comparisons adjusted for multiple hypothesis testing. Survival analyses were conducted in bulk RNA-seq and TMA cohorts using multivariable Cox proportional hazards models with Kaplan-Meier visualization.

Results

Anatomically Mapped Multisample Characterization of PM

Our workflow sampled multiple anatomically defined sites from PM surgical resections supporting characterization with scRNA-seq, bulk RNA-seq, and histopathology of adjacent tissue (Fig. 1*A* and Supplementary Fig. 1). We collected 93 samples from 40 patients: 20 ePM (19 with viable tumor), 13 bPM, three sPM, three non-PM pleura as controls for MC identification, and one incidental peripheral nerve sheath tumor (Supplementary Table 1A). In 36 PM cases, whole exome and OGM identified SNVs and CNVs, respectively. Mutations were consistent with previous PM studies (Fig. 1*B*; Supplementary Table 1B and C).[10,11,14,17] Multisite histopathology revealed substantial variation within and across tumors (Fig. 1*C*; Supplementary Table 1E). Adjacent bulk RNA-seq analysis confirmed consistency with previous molecular phenotypes (Supplementary Fig. 2A and B; Supplementary Table 1D).[9,11,13]

ScRNA-seq profiles of 266,262 cells (Supplementary Table 1F) were initially typed using dimensionality reduction-based clustering and marker gene analysis (UMIs $\geq$ 300, features $\geq$ 80) (Fig. 1*D*, Supplementary Figs. 3 and 4A and B, Supplementary Table 2). After restricting quality parameters further (UMIs $\geq$ 750, features $\geq$ 400), we used OGM-validated inferred CNVs to define clones in 136,910 high-quality cells (Fig. 1*E*, Supplementary Figs. 5 and 6; Methods). We robustly identified 32,383 MCs in these high-quality cells by combining cell phenotype, cluster patient specificity, inferred CNVs, and clonal assignment (Supplementary Fig. 4C–G; Methods). Separate analyses of stroma, immune, and MCs allowed us to parse TME components at high resolution (Supplementary Fig. 7A–C).

MC Expression Correlates With Bulk EM Gradient

Principal component analysis (PCA) of MC scRNA-seq profiles revealed EM gradient, extracellular matrix (ECM) composition, inflammation, and cell cycle as primary axes of variation (Supplementary Fig. 7D–G; Supplementary Table 3C). Published bulk histomolecular EM signature expression (Supplementary Table 3D[8–12]) was scored as described by Tirosh et al.[18] in MCs (Supplementary Fig. 7H–I). These scores correlated with principal component 1 (PC-1) (Supplementary Fig. 7H; R: -0.826, $p < 0.001$) and adjacent bulk RNA-seq signature expression (Supplementary Fig. 2C; R: 0.821, $p < 0.001$). This suggests that bulk EM gradient observations in PM reflect contributions from MCs[11] consistent with previous scRNA-seq analysis.[16]

As EM gradient correlated with PC-1, we identified 232 (high) and 371 (low) genes that correlated ($|r| > 0.15$) with PC-1 to define MC-derived S- and E-score signatures (henceforth, tS-score and tE-score), respectively (Fig. 2*A*; Supplementary Table 3E and F). Only 20 (46.5%) and 28 (63.6%) of expressed bulk Blum[9] S-score and E-score genes (Supplementary Table 3A) were present in tS and tE-score signatures, possibly reflecting nonmalignant contribution to bulk EM signatures. Orthogonal MC variation in PC-2 was related to ECM (Supplementary Fig. 8; Supplementary Table 4; Supplementary Results).

PM MCs Are Variably Committed to EM State

Some MCs expressed tE- and tS-score signatures equally at low levels (Supplementary Fig. 7J), which we termed "uncommitted." These cells were not outliers in terms of detected UMIs, genes, or mitochondrial transcripts and were detected in 27 of 28 patients (96.4%) with at least 50 MCs (Fig. 2*A* and *B*, Supplementary Fig. 9A). Uncommitted cells had intermediate PC-1 coordinates and low tE- and tS-scores suggesting low commitment to either phenotype (Fig. 2*C*). For all MCs, we computed a histo-commitment (HC) distance using scaled tE- and tS-score distance (Fig. 2*D*). We identified "uncommitted" MCs with HC distance less than 1.5 SDs below the mean (Fig. 2*A*–*D*). For simplicity of characterizing "uncommitted" cells, we refer to them as a distinct cell state, henceforth, recognizing that discerning stable versus transition state requires further investigation. MCs with positive and negative tE- and tS-score differences above the uncommitted state threshold were defined as "epithelioid" and "sarcomatoid" MC state, respectively.

An uncommitted (HC-score) gene signature was defined taking genes with low correlation to HC distance

within each row, where slide size indicates cellularity and color indicates % ePM. A blue star indicates that the examined slide is not immediately adjacent to scRNA-sequencing sample. Sites reflect anatomic mapping displayed in Figure 1*A*. (*D*) Lollipop plot displays the number of cells isolated (length) in each case, where shapes denote cells isolated by biologic sample (large circle) or technical replicate (small diamond). Shape fill indicates anatomic site of sample. Pie charts display the TME distribution observed across cases. (*E*) CNV structure of PM clones as inferred by inferCNV and associated OGM DNA samples of the same case, where observations are binned 10 kb genome windows.

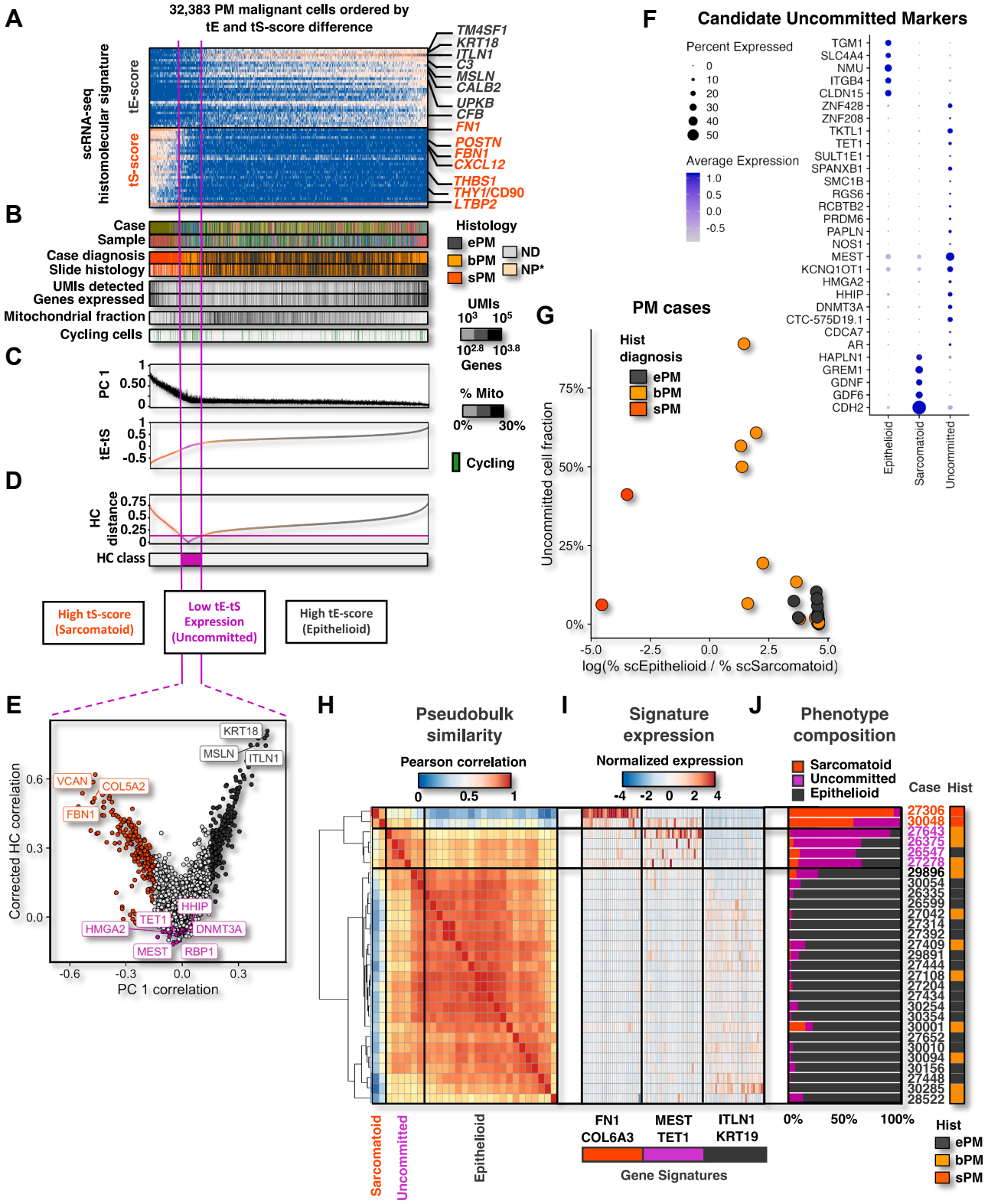

Figure 2. MCs in PM are variably committed to EM cell fate. (*A* and *B*) scRNA-seq histomolecular signature scores (*A*) and cell phenotype features (*B*) for 32,383 high-quality inferred CNV-confirmed MCs ordered by the difference of Blum E- and S-scores. (*C*) Scaled principal component (PC) 1 and scRNA-seq EM scores for individual MCs. (*D*) Histomolecular commitment (HC) distance and classification for MCs. Horizontal line denotes distance threshold for uncommitted MC state assignment (*E*) Relationship between gene expression correlation to corrected HC distance and PC1. Genes colored by MC state signature.

removing those expressed in more than 20% of sarcomatoid or epithelioid MCs to exclude sarcomatoid- and epithelioid-associated genes (Fig. 2*E*, Supplementary Table 3G; Methods). Uncommitted signature genes included *MEST*, *DMNT3A*, *TET1*, and *HHIP* (Fig. 2*E* and *F*; Supplementary Table 3G).

Among 2381 uncommitted cells obtained from samples with at least 50 MCs, 1731 (72.7%) were isolated from bPM tumors and 433 (18.2%) were actively cycling (Supplementary Fig. 9A–C). Samples with higher uncommitted cell fraction had similar epithelioid/sarcomatoid cell proportions (Supplementary Fig. 9D). High uncommitted cell fraction tumors were mostly bPM (Fig. 2*G*). ScRNA-seq epithelioid/sarcomatoid MC fraction correlated ($R = 0.787$, $p = 2.81 \times 10^{-9}$) with histopathologic sarcomatoid/epithelioid content estimations in adjacent slides (Supplementary Fig. 9E). We assigned adjacent bulk RNA-seq samples to four published molecular clusters[11]; most samples with intermediate epithelioid/sarcomatoid components in corresponding histologic and scRNA-seq analysis were in cluster 3(BS) (Supplementary Fig. 2D). Tumor samples in molecular clusters 3(BS) and 4(S) exhibited the highest uncommitted fraction in adjacent tissue scRNA-seq (Supplementary Fig. 2E).

Across patients, aggregated MC scRNA-seq expression clustered into three pseudo-bulk states, expressing predominantly either sarcomatoid, uncommitted, and epithelioid MC programs (Fig. 2*H* and *I*). These clusters corresponded to MC state fraction (Fig. 2*J*). To assess MC state variation within patients, individual site samples were similarly classified by predominant pseudo-bulk state (Supplementary Fig. 10A–D). Pseudo-bulk state correlated most strongly within patients (Supplementary Fig. 10E). Only four patients had sites assigned to more than one pseudo-bulk state.

Bulk RNA-Seq Identifies Candidate Biomarkers for MC State

After identifying three distinct MC state expression patterns, we hypothesized that candidate transcript biomarkers from MC state signature genes could identify predominant MC state in bulk RNA-seq. Using adjacent bulk and scRNA-seq tissue samples, we created and validated approaches using single sample gene set enrichment analysis (ssGSEA)[19] to assign predominant MC state to bulk RNA-seq samples using malignant exclusive signatures (meHCscore, meSscore, and meE-score) designed to exclude genes expressed by nonmalignant TME components (Supplementary Fig. 11A–D; Supplementary Table 5). Resulting assignments were 78.4% concordant with adjacent scRNA-seq analysis (Supplementary Fig. 11E and F).

We assessed biomarker expression in scRNA-seq adjacent bulk tissue samples with assigned MC state and associated with EM gradient operationalized by two-gene ratio of *CLDN15* and *VIM* (CV score).[11,13] We evaluated *MEST*, *THBS2*, and *MSLN* as candidate transcript biomarkers for predominantly uncommitted, sarcomatoid, and epithelioid samples, respectively. Uncommitted MC state tumors had higher *MEST* expression than epithelioid tumors (Supplementary Fig. 12A, $p = 0.027$). *MEST* was sensitive, identifying all uncommitted patients, but not specific given high expression in a subset of committed-rich cases (Supplementary Fig. 12B) with intermediate CV scores (Supplementary Fig. 12C). Even in low uncommitted samples, *MEST* may be a biomarker for mixed MC state tumors. *MSLN* was higher in epithelioid MC state tumors compared with sarcomatoid ($p = 0.0067$) or uncommitted ($p = 0.0043$) (Supplementary Fig. 12D). Epithelioid fraction (R^2: 0.57) and CV score (R^2: 0.66) positively correlated (Spearman) with *MSLN* expression (Supplementary Fig. 12E and F). *THBS2* did not discriminate sarcomatoid MC state at case or cell level (Supplementary Fig. 12G and H) though *THBS2* trended negatively with CV score (Supplementary Fig. 12I).

To validate RNA expression biomarkers in additional samples, as with adjacent bulk samples, we assigned 211 published bulk profiles[11] to predominant MC state using malignant exclusive signatures (Supplementary Fig. 11G; Methods). *MEST* bulk RNA-seq expression was higher in uncommitted predominant tumors (Supplementary Fig. 13A) compared with sarcomatoid ($p = 2.7 \times 10^{-4}$) and epithelioid ($p = 6.2 \times 10^{-6}$). *MSLN* expression was higher in epithelioid tumors (Supplementary Fig. 13B) compared with uncommitted ($p = 1.5 \times 10^{-7}$) or sarcomatoid ($p = 1.1 \times 10^{-9}$). Uncommitted ($p = 0.026$) or sarcomatoid ($p = 7.7 \times 10^{-4}$) MC state tumors expressed more *THBS2* than epithelioid tumors (Supplementary Fig. 13C). *MEST* expression was highest for intermediate CV score tumors (Supplementary Fig. 13D and E), but CV

(*F*) Candidate uncommitted marker gene expression by MC type with representative tE- and tS- signature genes, where fraction of cell expressing gene and expression level is annotated by size and shade, respectively. (*G*) Uncommitted MC fraction relationship with log ratio epithelioid/sarcomatoid MC state fraction in each case. Case diagnosis is annotated by color. (*H*) Hierarchically clustered correlation of mean aggregated expression of scRNA-seq MC state signatures for each PM case (rows and columns). (*I*) Mean aggregated expression of scRNA-seq MC state signature genes (columns) for each PM case (rows). (*J*) Composition of each PM case by MC state. Case histology diagnosis is annotated by color to the right. Histology diagnosis and adjacent slide histology annotation are as follows: ePM, epithelioid histology; sPM, sarcomatoid histology; bPM, biphasic histology; NP*, no MCs on adjacent histology slide; ND, no adjacent histology analysis available.

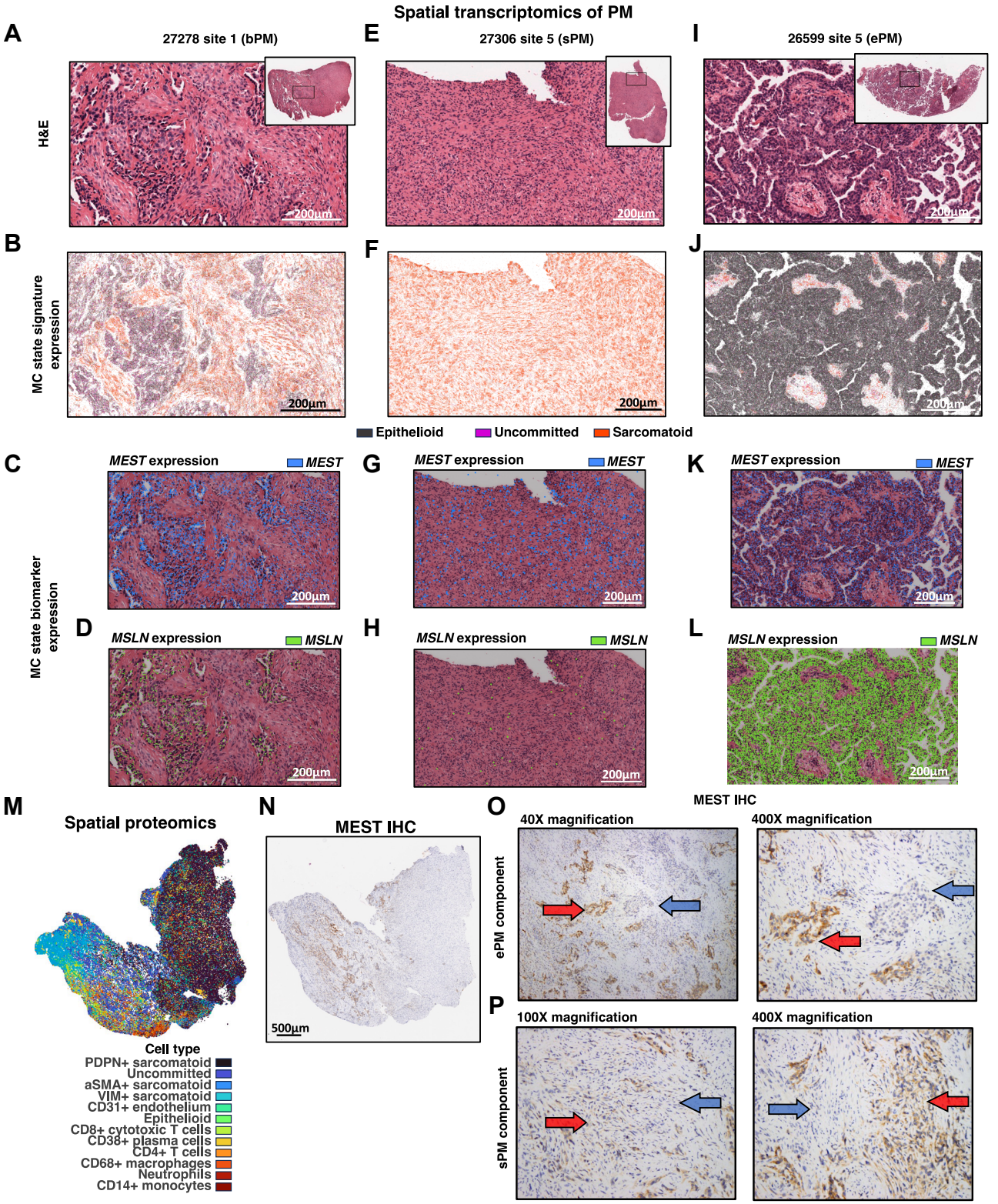

Figure 3. MC-state and associated biomarkers validated in spatial "omics." (*A*–*L*). Spatial transcriptomics analysis of bPM sample 27278 site 1 (*A*–*D*), sPM sample 27306 site 5 (*E*–*H*), and ePM sample 26599 site 5 (*I*–*L*). For each sample, the H&E (*A*, *E*, *I*), aggregate expression of MC state signature genes (*B*, *F*, *J*), and biomarker expression of MEST (*C*, *G*, *K*) and MSLN (*D*, *H*, *L*) individual transcripts are found. (*M* and *N*) Additional tissue level of 27278 site 1 tissue analyzed with Akoya phenocycler spatial transcriptomics (*M*) or MEST IHC stain (*N*). (*O* and *P*) Exemplar MEST IHC in ePM (*O*) and sPM (*P*) samples illustrating

score correlated (Spearman) positively (R^2: 0.39) with *MSLN* (Supplementary Fig. 13F) and negatively (R^2: 0.394) with *THBS2* (Supplementary Fig. 13G). These observations suggest that *MEST* and *MSLN* are robust biomarkers of uncommitted and epithelioid MC state, respectively.

Spatial "Omics" Validates MC State and Associated Biomarkers

Using spatial transcriptomics, we measured expression in situ of 477 genes (Xenium Human Immuno-oncology panel including 100 custom genes incorporating MC state signatures) (Supplementary Table 6A) in seven samples from four PM patients (Methods) to validate MC state and candidate biomarkers. We identified 34 clusters of 628,968 cells (Supplementary Fig. 14A and B). Using scType,[20] clusters were mapped to all MC states and expected non-MCs, including macrophages, monocytes, fibroblasts, CD4+, and CD8+ T cells among others (Supplementary Fig. 14C–E). MC state was concordant between spatial and scRNA-seq analyses (Supplementary Fig. 15A).

In bPM (case 27278), spatial transcriptomics identified uncommitted cells within epithelioid morphology components that expressed uncommitted, epithelioid, and sarcomatoid signatures (Fig. 3*A* and *B*, Supplementary Fig. 15B). *MEST* expression was high in epithelioid morphology components of bPM case 27278 (Fig. 3*C*), whereas MSLN expression was low but present (Fig. 3*D*). In contrast, sPM (case 27306; Fig. 3*E* and *F*, Supplementary Fig. 15D) and ePM (case 26599; Fig. 3*I* and *J*, Supplementary Fig. 15C) histology samples only exhibited sarcomatoid and epithelioid signatures, respectively. Biomarker expression accurately delineated MC state, where sPM was $MEST_{low}$ and $MSLN_{low}$ (Fig. 3*G* and *H*) and ePM with low adjacent scRNA-seq uncommitted cell fraction was $MEST_{low}$ and $MSLN_{high}$ (Fig. 3*K* and *L*). These data validate uncommitted MC state and reinforce the utility of MC state biomarkers, *MEST* (uncommitted) and *MSLN* (epithelioid).

We evaluated MEST expression using spatial proteomics and IHC of seven adjacent exemplar slides. Using a 51-gene spatial proteomics panel (Akoya Phenocycler) (Supplementary Table 6B; Methods), we found analogous cell types (Fig. 3*M*). One cluster expressed epithelioid and sarcomatoid markers, which we annotated as uncommitted. Using adjacent tissue, we observed high MEST expression in these putative uncommitted cells (Fig. 3*N*). In exemplar MEST-stained IHC tissue, MEST+ cells exhibited substantial morphologic heterogeneity (Supplementary Fig. 16; Supplementary Results) and varied within samples with strong or absent staining in distinct subpopulations (Fig. 3*O* and *P*). These findings characterize MEST+ morphology and validate uncommitted phenotype in protein assays identifying MEST as a candidate uncommitted state IHC biomarker.

TME Comprises Diverse Stromal and Immune Types

To characterize TME and potential associations with MC state, we separately clustered high-quality stromal (10,659) and immune (50,309) cells. We observed expected stromal populations, including mesothelial, fibroblast, endothelial, vascular smooth muscle, alveolocyte, adipocyte, and pericyte cells (Supplementary Fig. 17; Supplementary Table 7; Supplementary Results). Twelve distinct fibroblast subpopulations were identified. *TGFBI* and *IGF1* were top marker genes discriminating fibroblast subsets. Expected immune populations, including B, mast, macrophage, monocyte, dendritic, CD8+ T, CD4+ T, natural killer, and Treg cells, were isolated (Supplementary Fig. 18; Supplementary Table 8; Supplementary Results). Three distinct macrophage subpopulations were observed delineated by *SEPP1*, *SPP1*, or *IFIT1* marker genes.

PM Tumor Microenvironment Varies With MC State

Distinct immune and histopathologic axes of variation have been proposed with multiomics analysis.[14] To determine how TME varies with MC state, we clustered 60 PM scRNA-seq samples with at least 200 non-MCs by cell type fraction. This segregated tumors into TME niche groups with distinct pseudo-bulk MC states (Supplementary Fig. 19A and B). Uncommitted MC state was significantly enriched for exhausted CD8+ T cells (niche 4). Epithelioid MC state was significantly depleted in Treg cells but enriched in IFN receptor positive CD8+ T (IFNr CD8) and NK (NKCs) cells (niches 1 and 2), whereas sarcomatoid MC state (niche 7) was enriched in *CXCL8*+ TAM (Supplementary Fig. 19A–C). TME was consistent across sampled sites (Supplementary Fig. 19D).

Because TME fraction segregated MC state, we hypothesized that TME features such as macrophage fraction and fibroblast type may vary with MC state. Macrophage TME fraction trended lower in uncommitted samples (Supplementary Fig. 19E). Fibroblast subtype composition significantly varied with MC state (Fig. 4*A*). Uncommitted and sarcomatoid samples contained more *TGFBI*+ fibroblasts than epithelioid samples, especially relative to

heterogeneity of MEST staining with MEST+ and MEST− cells emphasized with red and blue arrows, respectively. Malignant state signatures consist of scRNA-seq signatures (epithelioid: meEscore, uncommitted: meHCscore, sarcomatoid: meS-score), operationalized with custom Xenium panel.

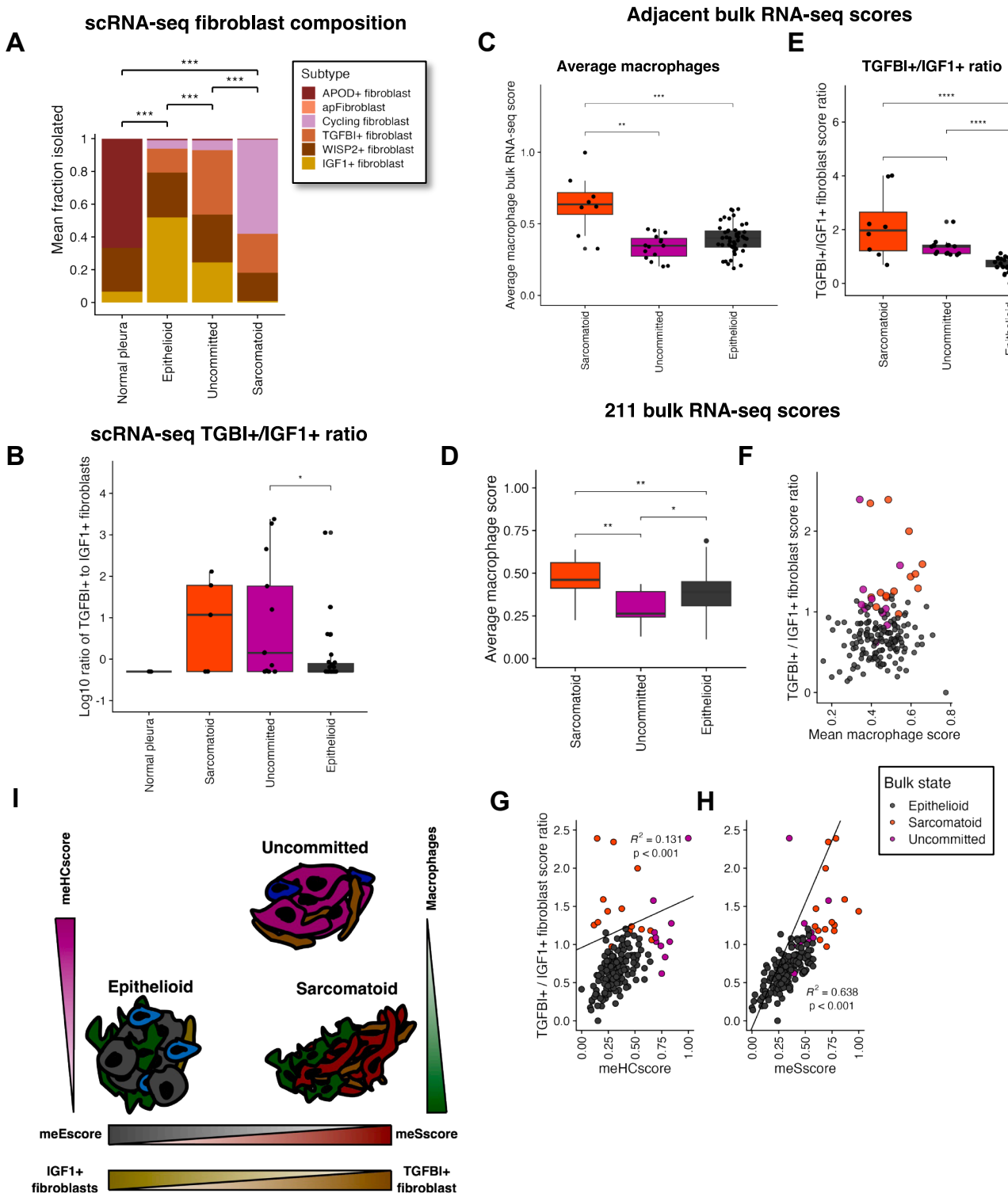

Figure 4. Non-MCs in the TME associate with MC state. (*A*) Average fraction of each fibroblast subtype with respect to total fibroblasts isolated in each sample for each MC state and non-PM pleura. Asterisks indicate adj. *p* value less than 0.001 with Fisher's exact test. (*B*) Log10 TGFBI+/IGF1+ fibroblast ratio in scRNA-seq samples. (*C*, *E*) Average macrophage signature score (*C*) or TGFBI+/IGF1+ fibroblast signature score ratio (*E*) in adjacent bulk RNA-seq for each assigned MC-state. (*D*, *F*-*H*) Analysis of independent 211 bulk RNA-seq samples with assigned MC state depicts average macrophage score by MC state (*C*), relationship between *TGFBI+/IGF1+* fibroblast ratio and average macrophage score (*D*), and correlation of *TGFBI+* to *IGF1+* fibroblast ratio with malignant exclusive uncommitted (meHCscore) (*E*) or sarcomatoid (meSscore) (*F*) MC state signatures. Assigned bulk MC state is annotated by color. (*I*) Model of PM TME association with MC state. In all boxplots, *p* values are displayed for statistical comparison with Wilcoxon ranked sum test and annotated as $p < 0.05$ (*), $p < 0.01$ (**), $p < 0.001$ (***), and $p < 0.0001$ (****).

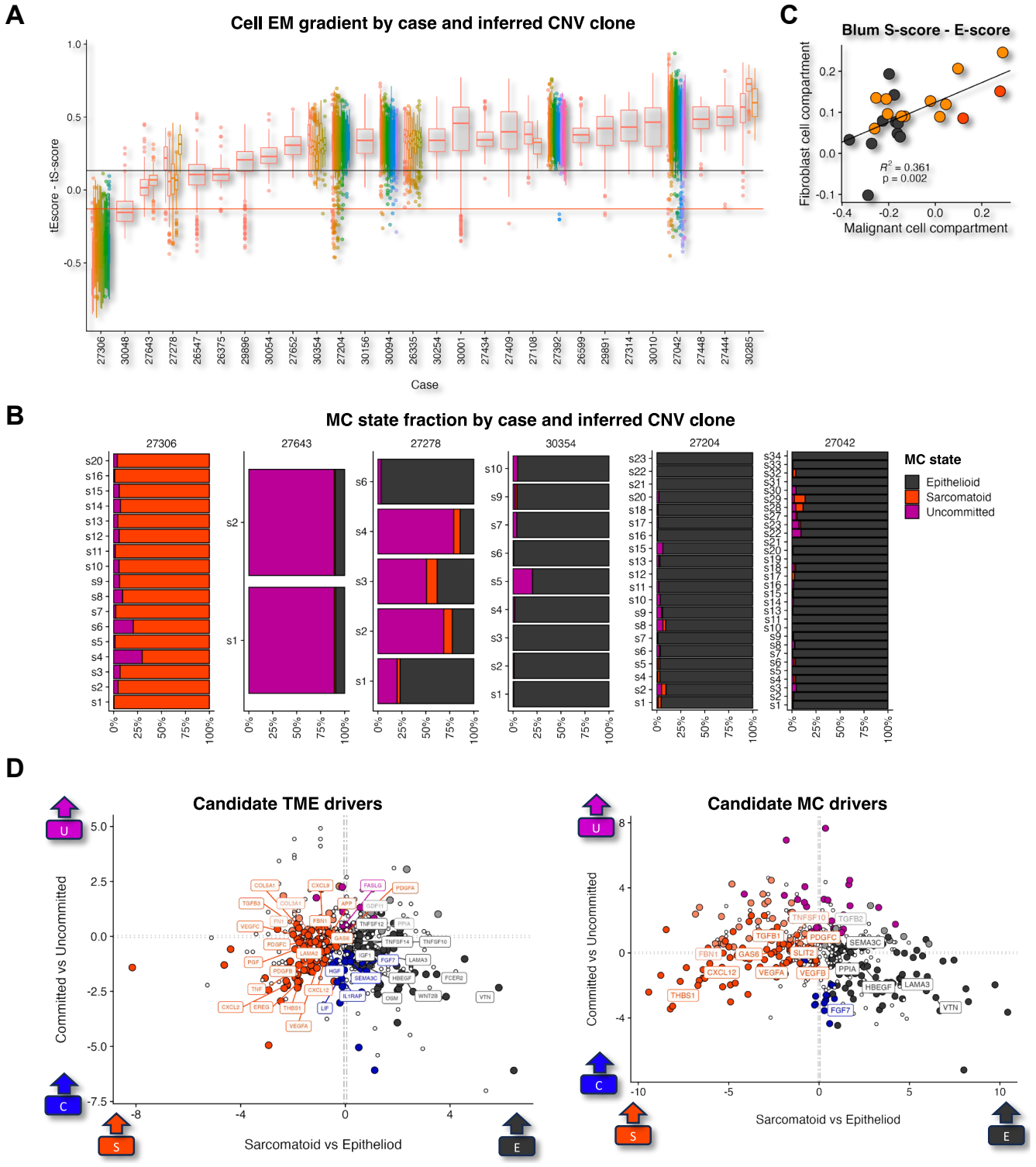

Figure 5. EM gradient in PM is not clonal and candidate TME drivers associate with MC state. (*A*) scRNA-seq EM gradient score distribution of MCs across PM cases and clones. Box outline displays scRNA-seq inferred CNV clone within each case. Horizontal lines annotate thresholds for epithelioid (dark grey) and sarcomatoid (orange red) MC state. (*B*) Proportion of cells in each MC state within distinct clones identified in six representative PM cases of 11 PM cases with more than one subclone identified. (*C*) Correlation of Blum EM gradient signature expression between fibroblast and MC tumor cell compartments. (*D* and *E*) Candidate non-MC TME (*D*) and MC intrinsic (*E*) genes differentially expressed in non-MCs (*D*) or MCs (*E*) between tumors assigned to distinct MC pseudo-bulk states. Labeled genes were identified as having significant TME interactions using CellPhoneDB and filtered for public annotation as extracellular signals. Color-coded schema indicates whether up-regulation is in uncommitted (U), committed (C), sarcomatoid (S), or epithelioid (E).

IGF1+ fibroblasts (Fig. 4*B*; $p < 0.05$). We again leveraged adjacent bulk RNA-seq samples to create and evaluate non-MC type signatures scored with ssGSEA[19] and assessed for accurate TME cell fraction quantification in bulk tissue (Supplementary Fig. 20; Supplementary Table 5; Methods). Thirty cell type quantifications of adjacent bulk samples correlated ($R \geq 0.10$) with scRNA-seq cell fraction (Supplementary Fig. 20A–D). As in scRNA-seq data, clustering on quantified TME fractions segregated MC-state in adjacent bulk tissue (Supplementary Fig. 20E) and independent 211 cohort (Supplementary Fig. 21).

Cell type quantification in adjacent and independent bulk RNA-seq validated scRNA-seq findings. Bulk uncommitted tumors had significantly lower macrophage scores than sarcomatoid tumors (Fig. 4*C* and *D*). Bulk analysis also validated higher *TGFBI*+ to *IGF1*+ fibroblast score ratio for non-epithelioid MC state tumors in adjacent samples (Fig. 4*E*; $p < 0.001$) and in the 211 cohort (Fig. 4*F*–*H*). Concordantly, bulk and scRNA-seq analysis demonstrate distinct TMEs associated with MC state; uncommitted tumors exhibited fewer macrophages, and epithelioid tumors were enriched for *IGF1*+ compared with *TGFBI*+ fibroblasts (Fig. 4*I*).

EM Gradient Is Not Clonal in PM

We evaluated EM score in MCs across individual clones using "inferCNV" to identify CNV alterations and assign MCs into clones with distinct CNVs (Fig. 1*E*, Supplementary Fig. 6A). Many samples appeared monoclonal, but 11 tumors exhibited multiple subclones. Using OGM, we identified deletions in 3p, 9, 13, 14, and 22 consistent with previous studies (Supplementary Fig. 6B). Clustering OGM-derived CNV profiles with clonal scRNA-seq inferCNV profiles demonstrated similar CNV features and co-clustering of sample/clones primarily by case (Fig. 1*E*, Supplementary Fig. 6C). Average Spearman correlation was higher (paired *t* test: $p < 0.001$) between OGM and inferCNV profiles within (R: 0.52) than between patients (R: 0.16) (Supplementary Fig. 22A).

We hypothesized that distinct MC clones would segregate by MC state in heterogeneous PM tumors. However, we observed no relationship between MC state and CNV clone. Although cell EM gradient (tE – tS score) was restricted by patient, it did not vary by inferred CNV clone (Fig. 5*A*). Individual clones often comprised two or three MC states (Fig. 5*B*, Supplementary Fig. 22B). In one uncommitted biphasic case, five of six OGM-confirmed clones expressed all three MC states (Supplementary Fig. 22C and D). Thus, MC state is not restricted by specific CNV clones and varies among cells with shared CNVs.

We hypothesized factors within the TME may drive EM cell state. We found that Blum EM gradient[9] of patients' MC and fibroblast components correlated with one another (Fig. 5*C*; R^2: 0.361). Across samples, MC EM gradient also correlated with fibroblasts (Supplementary Fig. 22E; R^2: 0.387), all stromal cells (Supplementary Fig. 22F; R^2: 0.401), but not immune cells (Supplementary Fig. 22G; R^2: 0.025). EM gradient may be a shared property of MC and stromal tumor components due to TME drivers.

TME Factors Associate With EM Gradient

To identify candidate TME drivers of MC state, we compared extracellular signal expression between tumors predominated by each MC state using differential expression analysis. To parse drivers expressed by non-MCs in the TME and those expressed by MCs themselves, we contrasted signal expression separately in nonmalignant (Fig. 5*D*; Supplementary Table 9A) and malignant (Fig. 5*E*; Supplementary Table 9B) cells. We further narrowed candidate drivers with "CellPhoneDB"[21] filtering for significant MC-MC or non-MC-MC interactions (Supplementary Table 9C).

Sarcomatoid MC state was associated with TME expression of *TGFB3* and *GAS6* signals (Fig. 5*D* and *E*; Supplementary Table 9D). *TGFB3* interacted with *TGFB1* receptor and was expressed by pericytes, vascular smooth muscle cells, and *WISP2*+ or *TGFBI*+ fibroblasts (Supplementary Fig. 23A and B). *GAS6* was expressed by sarcomatoid cells, dendritic cells, and *SEPP1* TAMs and interacted with *AXL* receptor in sarcomatoid MCs. Spatial transcriptomics demonstrated highest *AXL* expression in sarcomatoid regions, whereas macrophage-dense regions exhibited high *GAS6* expression in sPM case 27306 (Supplementary Fig. 15E, Supplementary Fig. 23C and D; $p < 0.001$). This suggests potential co-dependence of distinct TME niches. In the 211 cohort, *AXL* expression was significantly elevated in sarcomatoid histology and MC state (Supplementary Fig. 23E), but *GAS6* was variable (Supplementary Fig. 23F).

Epithelioid MC state tumors were notable for *HBEGF* expression mediated by *EGFR* and expressed ubiquitously by myeloid cell types (Supplementary Fig. 23A and B; Supplementary Table 9E). Epithelioid MCs had higher *WNT2B* expression (Supplementary Fig. 23G; $p < 0.0001$), whereas uncommitted and sarcomatoid cells expressed WNT inhibitory receptors *SFRP2* and *SFRP4*, respectively. Decreased WNT signaling could explain down-regulation of beta-catenin in more mesenchymal MCs.[22] Together, these findings identify candidate drivers of PM state for further exploration in murine and ex vivo organoid models.

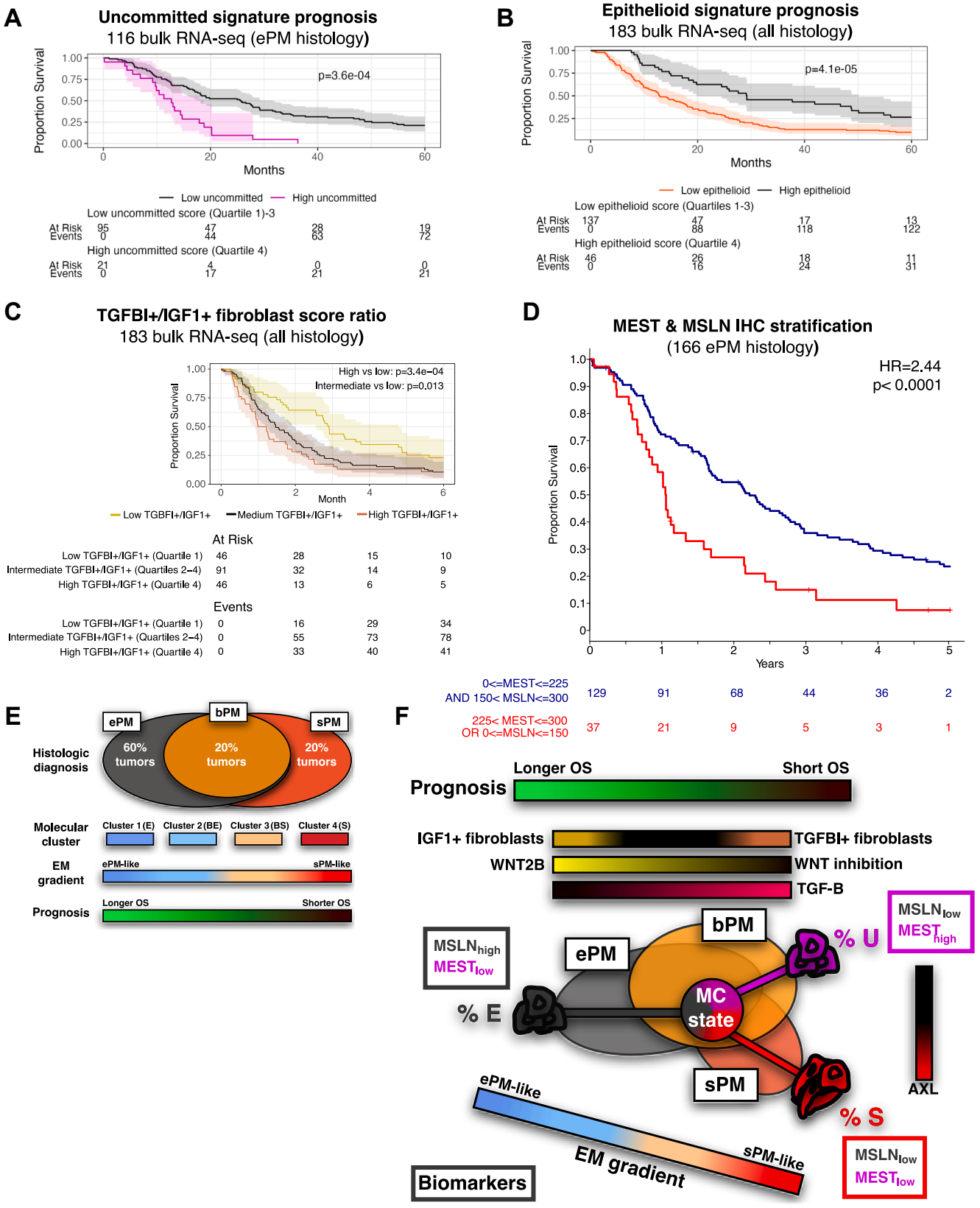

Figure 6. An updated model of PM microenvironment, heterogeneity, and prognosis. (*A* and *B*) Kaplan-Meier survival curves and at-risk tables display overall survival stratified by quartile 4 versus 1 to 3 uncommitted meHC-score signature expression in 116 ePM bulk RNA-seq patients (*A*), quartile 4 versus 1 to 3 epithelioid meE score signature expression in 183 bulk RNA-seq patients (*B*), quartile 1 versus 2 to 3 versus 4 TGFBI+/IGF1+ signature scores in 183 bulk RNA-seq patients (*C*). (*D*) Kaplan-

MC State and Associated TME Are Prognostic in PM

In 183 independent bulk RNA-seq samples, uncommitted score stratified survival in ePM patients (Fig. 6*A*; $p = 3.6 \times 10^{-4}$) but did not significantly stratify all patients (Supplementary Fig. 24A). Epithelioid score was associated with positive prognosis in all patients (Fig. 6*B*; $p = 4.1 \times 10^{-5}$) and those with ePM histology (Supplementary Fig. 24B). Both low *MEST* (Supplementary Fig. 24C and D) and high *MSLN* (Supplementary Fig. 24E and F) expression associated with significantly longer overall survival in ePM patients. Because fibroblast composition, especially *TGFBI*+ to *IGF*1+ fibroblast ratio, was associated with MC state, we hypothesized that it may stratify overall survival. Among ePM tumors, intermediate and high *TGFBI*+ to *IGF*1+ fibroblast ratio conveyed progressively worse prognoses (Fig. 6*C*; $p < 0.05$). Thus, MC state, associated biomarkers, and fibroblast TME can stratify patients beyond traditional histologic classification.

We optimized existing antibodies and designed four TMAs to include 290 patients with representative histology who underwent extirpative surgery followed by chemotherapy (ePM: 166, sPM: 7, bPM: 117) for MEST and MSLN staining and subsequent scoring with an H-score to assess MC state biomarker association with histology and prognosis.[23] In expanded TMA analysis of 452 patients, MEST and MSLN expression significantly differed by histotype (Supplementary Fig. 25A and B; Supplementary Results). High MEST was associated with shorter OS in ePM tumors (Supplementary Fig. 25C; HR: 3.01, $p = 6 \times 10^{-4}$). MSLN IHC was associated with longer OS in ePM and bPM tumors (Supplementary Fig. 25D; HR: 0.44, $p = 3 \times 10^{-4}$) and ePM tumors alone (Supplementary Fig. 25E; HR: 0.49, $p = 0.008$). Combined MEST and MSLN IHC stratified ePM tumors with 13-month versus 27-month median survival (Fig. 6*D*; HR: 2.44, $p < 0.0001$).

scRNA-seq and Spatial Transcriptomics Inform a New PM Prognostic Approach

Bulk studies[9,11,24] previously described a continuous histopathologic gradient model, where histology associated with molecular features but with frequent exceptions (Fig. 6*E*). All four described EM clusters contain ePM tumors (Supplementary Fig. 23E and F). Cluster 1(E) epithelioid tumors associated with better prognosis exhibited high epithelioid and low uncommitted MC state scores (Supplementary Fig. 26A). High sarcomatoid MC scoring ePM tumors found in clusters 2(BE), 3(BS), and 4(S) exhibit either high uncommitted MC state or fibroblast scores (Supplementary Fig. 26B and C). Thus, bulk analysis or histology may incorrectly prognosticate tumors due to infiltrating fibroblasts or discordance between morphology and MC state.

sPM, bPM, and ePM histology tumors each contain variable MC state fractions including newly described uncommitted state (Fig. 6*F*). WNT inhibition coupled with GAS6-AXL and TGF-β signaling are features of uncommitted and sarcomatoid MC state tumors. Thus, although histology and bulk EM stratification continue to be valuable prognostic factors, MC state and associated TME are critical novel axes of variation for prognosis and therapy response predictions. Furthermore, MEST and MSLN IHC biomarkers for MC state represent powerful new prognostic tools for stratifying patients.

Discussion

Using a large representative cohort of multisite PM samples, we demonstrate that previously described EM variation in bulk samples exists within MCs as reported in previous scRNA-seq work.[16] We newly describe an uncommitted MC state frequently identified in bPM samples. High uncommitted signature expression is correlated with worse prognosis in ePM and may be related to mixed, "cm14," signature described by Giotto et al., which was also associated with worse prognosis.[16] We demonstrate that individual MC states are not defined by distinct clones. This does not preclude genetic determinants of MC state but is evidence that distinct mutations are not required for MC state changes. By dissecting PM with scRNA-seq, we identify candidate drivers of proliferation and EMT expressed by both MCs and their surrounding microenvironment. Distinct TME components may interact to drive malignancy and modulation of nonmalignant signaling may provide new targets in PM or other cancers. Uncommitted, macrophage, and fibroblast cells express *GAS6*, thereby promoting proliferation in *AXL*-expressing sarcomatoid cells. *GAS6/AXL* signaling was previously described as an EMT factor in PM,[25,26] and *AXL* was recently described as associated with sarcomatoid module expression.[16] These data may direct precision

Meier survival curve and at-risk table displays overall survival stratified integrated MSLN/MEST IHC staining across 166 ePM patients in TMA cohort. *p* values represent the test of hazard ratio = 1 in multivariable Cox proportional model, including T stage, N stage, ECOG performance status, neoadjuvant chemotherapy (*A*, *D*), and histotype (ePM versus non-ePM) when analysis included all histotypes (*B* and *C*). (*E*) Previous bulk model of PM depicts prognostic histotype and bulk molecular EM gradient (discrete clusters and continuous spectrum). (*F*) Schematic of new model of PM integrating MC state and the TME, where biomarkers (boxes) delineate MC state prognostic subsets beyond histotype. bPM, biphasic histology; E, epithelioid MC state; ePM, epithelioid histology; S, sarcomatoid MC state; sPM, sarcomatoid histology; U, uncommitted MC state.

therapy nominating targets such as GAS6/AXL inhibition for sarcomatoid PM treatment.

Several limitations of this study should be noted. The candidate drivers identified as associated with MC state are observational. Knockout or overexpression experiments are needed to confirm genuine drivers of MC state. Our TME observations and validation rely on scRNA-seq and estimated bulk RNA-seq cell type quantification, respectively. Although frequently performed, these approaches can be inaccurate. Prospective flow cytometry cohorts could validate TME associations with MC state in further studies. Although our cohort spanned all histotypes, only three and eight sPM tumors underwent scRNA-seq analysis or TMA survival analysis, respectively. sPM is over-represented in our surgical cohort; however, sPM comprises approximately 10% to 20% of PM and is under-represented in these analyses. Although conclusions regarding bPM, ePM, and surgical PM are generalizable from our work, sPM under-representation may have limited power in gene, TME feature, and survival associations with sarcomatoid MC state.

Recent bulk analysis integrating DNA, RNA, and methylation "omics" in PM proposed four orthogonal axes for classification: ploidy, adaptive response, morphology, and methylation.[14] These factors capture diverse PM features but are difficult to implement clinically. Using annotated multisite scRNA-seq samples, we demonstrate diverse axes of variation in morphology, MC state, and associated TME. Further scRNA-seq and spatial analysis over larger patient cohorts could facilitate deeper exploration of MC state relationships with adaptive response or ploidy. This work demonstrates MC state and associated TME meaningfully stratify patients. Moreover, we identify two single protein IHC biomarkers of MC state, MEST and MSLN, which pending further validation can be readily adopted to augment existing diagnostics improving patient stratification for shared decision-making and clinical trial design. Thus, our findings have immediate prognostic and diagnostic implications in PM.

CRediT Authorship Contribution Statement

David T. Severson: Conceptualization, Validation, Formal analysis, Investigation, Data curation, Writing - original draft, Writing - reviewing & editing, Visualization, Project administration.

Samuel Freyaldenhoven: Conceptualization, Investigation, Writing - reviewing & editing.

Benjamin Wadowski: Investigation, Writing - reviewing & editing, Visualization.

Yin P. Hung: Investigation, Pathology, Writing - reviewing & editing.

Travis Hughes: Resources.

Beow Y. Yeap: Validation, Formal analysis.

William G. Richards: Conceptualization, Validation, Resources, Data curation, Writing - reviewing & editing.

Sanna Laaksonen: Pathology.

Lucian Chirieac: Pathology.

Matthew B. Couger: Formal analysis, Resources.

Roderick V. Jensen: Formal analysis, Investigation, Writing - reviewing & editing.

Ahmed A. Sadek: Validation, Resources, Data curation.

Ilkka Ilonen: Resources, Data curation.

Kimberly Vermilya: Resources, Data curation.

Simona Innocenti: Resources, Data curation.

Stephanie L. Korle: Resources.

Julianne S. Barlow: Resources.

Jamie Anderson: Resources.

Jason Meyerovitz: Resources.

Vivian Wang: Investigation, Resources.

Mary N. Dao: Resources.

Alex K. Shalek: Writing - reviewing & editing, Supervision.

Assunta De Rienzo: Conceptualization, Resources, Data curation, Writing - reviewing & editing.

Raphael Bueno: Conceptualization, Writing - reviewing & editing, Supervision, Project administration, Funding acquisition.

Disclosure

Dr. Hung discloses that he receives royalties from Elsevier and American Society of Clinical Pathology for textbook writing and continuing medical education (CME) activities, respectively. Neither activity is related to this manuscript. Dr. Shalek reports receiving compensation for consulting and/or having SAB membership from Merck, Honeycomb Biotechnologies, Cellarity, Repertoire Immune Medicines, Hovione, Third Rock Ventures, Ochre Bio, FL82, Empress Therapeutics, Relation Therapeutics, Senda Biosciences, IntrECate Biotherapeutics, Santa Ana Bio, and Dahlia Biosciences unrelated to this work. Dr. Shalek has received research support from Merck, Novartis, Leo Pharma, Janssen, the Bill and Melinda Gates Foundation, the Moore Foundation, the NIH, the Moore Foundation, Wellcome Leap, the Pew-Stewart Trust, Foundation MIT, the Chan Zuckerberg Initiative, Novo Nordisk, and the Food and Drug Administration unrelated to this work. Dr. Bueno reports receiving research funding from NCI, NIBIB, NHLBI, DOD, and from Early, Serum, Bicycle Therapeutics, Genentech, Roche (ImCORE), Merck, Siemens, Verastem, and Intuitive Surgical, in addition to philanthropic funds from the IMP. Also, patents were licensed through BWH and equity in Navigation Sciences (a surgical device company). The remaining authors declare no conflict of interest.

Acknowledgments

This work was supported by the International Mesothelioma Program and its donors at Brigham and Women's Hospital. In particular, the authors acknowledge substantial donations from Richard and Madé Berg, Mark and Cindy Blotner, Celani Family Foundation, Anne Favell Mesothelioma Research Fund, Kim Scott, Mike and Amy Thornton, Cuiyan Yang, and Shunli Zheng. It was also supported by R01 funding of Dr. Raphael Bueno from the National Cancer Institute. The authors are grateful to the patients who consented to have their tissues studied herein and made this work and resulting manuscript possible. The study sponsors played no role in the study design, collection, analysis, interpretation of data, writing of the report, or decision to submit the paper for publication. Dr. David T. Severson would like to thank the American Cancer Society, American Association for Thoracic Surgery, and the National Cancer Institute for support provided by the American Cancer Society Post-doctoral Fellowship (PF-24-1314966-01-MM, https://doi.org/10.53354/ACS.PF-24-1314966-01-MM.pc.gr.222109), David J Sugarbaker Surgical Resident Investigator, and Duke Surgical Oncology T32 awards, respectively.

Data Availability Statement

Raw FASTQ files for bulk, scRNA-seq, OGM, and exome data will be made available for download with appropriate controlled access for primary patient specimen on SRA via dbGaP before publication (SRA accession pending). Raw and normalized counts for bulk and scRNA-seq data and raw OGM data will be made available on GEO before publication (GEO accession pending). Annotations for bulk and scRNA-seq case, samples, and cells are found in Supplementary Table 1. A complete list of resulting SNV and CNVs called from exome and OGM analysis, respectively, are also found in Supplementary Table 1. The reads for 211 previously published PM bulk RNA-seq profiles[11] used in this study are available at the European Genome-phenome Archive under accession code EGAS00001001563.

Code Availability Statement

Publicly available and commercial packages were used for data collection as outlined by the methods in detail. For scRNA-seq data, raw reads were processed into counts using publicly available DropSeq tools[27] pipeline. Bulk RNA-seq data were mapped to hg38 using publicly available STAR version 2.7.3[28] and GENCODE v28 annotation. CNVs were identified from OGM data using Bionano Access Version 1.6 and 1.7 rare variant (>5000 bp) and copy number (>500,000 bp) pipelines, which are available from BioNano. Exome sequencing libraries from each case were concatenated using the Seven Bridges SBG FASTQ Merge CWL v.1.0 tool. For spatial transcriptomics, data were acquired on the Xenium analyzer and software while count matrixes produced by the Xenium were processed with the squidpy analysis suite[29] and in R (v.4.3.2).

Data analysis was performed with publicly available code and software. Briefly, scRNA-seq data were processed using best practices with publicly available Seurat (v.4.0.1).[30] CNVs were inferred form scRNA-seq data using the publicly available inferCNV.[31–33] Downstream analysis in R (v.4.3.2), including plot and scRNA-seq scores generation, was performed with custom code implementing methods introduced by Tirosh et al.[18,34] available upon request. For bulk RNA-seq data, differential expression analysis was performed with edgeR[35,36] Bulk RNA-seq signature scores were computed with the GSVA package[37] available in Bioconductor. Downstream analyses of bulk RNA-seq data were performed with standard publicly available R packages as described in the methods. All R code for QC-analysis, cell type assignment, inferCNV analysis, signature generation, score computation, and plot generation is readily available upon request.

Exome SNVs were called using Seven Bridges "WES Tumor-Normal with Variant Calling, CNV estimation, TMB, MSI and HRD scores" public application (sgb:draft-2, v.1.0) developed by PDXNet. For both OGM and SNV analyses, figures visualizing resulting SNVs and CNVs were generated in R and custom code for figure plots is available upon request. Downstream clustering and plotting of spatial transcriptomics data were performed using publicly available Seurat (v.4.0.1).[30] For spatial proteomics, a publicly available custom R package from Enable Medicine (https://docs.enablemedicine.com/spatialmap) was used for data normalization, cell phenotyping, and data visualization.

Supplementary Data

Note: To access the supplementary material accompanying this article, visit the online version of the *Journal of Thoracic Oncology* at www.jto.org and at https://doi.org/10.1016/j.jtho.2025.11.019.

References

1. Peto J, Seidman H, Selikoff IJ. Mesothelioma mortality in asbestos workers: implications for models of carcinogenesis and risk assessment. *Br J Cancer*. 1982;45:124–135.
2. Sekido Y. Molecular pathogenesis of malignant mesothelioma. *Carcinogenesis*. 2013;34:1413–1419.
3. Carbone M, Adusumilli PS, Alexander HR Jr, et al. Mesothelioma: scientific clues for prevention, diagnosis, and therapy. *CA Cancer J Clin*. 2019;69:402–429.
4. Bou-Samra P, Chang A, Azari F, et al. Epidemiological, therapeutic, and survival trends in malignant pleural

mesothelioma: a review of the National Cancer Database. *Cancer Med*. 2023;12:12208–12220.
5. Yap TA, Aerts JG, Popat S, Fennell DA. Novel insights into mesothelioma biology and implications for therapy. *Nat Rev Cancer*. 2017;17:475–488.
6. Nowak AK, Jackson A, Sidhu C. Management of advanced pleural mesothelioma-at the crossroads. *JCO Oncol Pract*. 2022;18:116–124.
7. Baas P, Scherpereel A, Nowak AK, et al. First-line nivolumab plus ipilimumab in unresectable malignant pleural mesothelioma (CheckMate 743): a multicentre, randomised, open-label, phase 3 trial. *Lancet*. 2021;397:375–386.
8. Alcala N, Mangiante L, Le-Stang N, et al. Redefining malignant pleural mesothelioma types as a continuum uncovers immune-vascular interactions. *EBiomedicine*. 2019;48:191–202.
9. Blum Y, Meiller C, Quetel L, et al. Dissecting heterogeneity in malignant pleural mesothelioma through histo-molecular gradients for clinical applications. *Nat Commun*. 2019;10:1333.
10. Hmeljak J, Sanchez-Vega F, Hoadley KA, et al. Integrative molecular characterization of malignant pleural mesothelioma. *Cancer Discov*. 2018;8:1548–1565.
11. Bueno R, Stawiski EW, Goldstein LD, et al. Comprehensive genomic analysis of malignant pleural mesothelioma identifies recurrent mutations, gene fusions and splicing alterations. *Nat Genet*. 2016;48:407–416.
12. de Reyniès A, Jaurand MC, Renier A, et al. Molecular classification of malignant pleural mesothelioma: identification of a poor prognosis subgroup linked to the epithelial-to-mesenchymal transition. *Clin Cancer Res*. 2014;20:1323–1334.
13. Severson DT, De Rienzo A, Bueno R. Mesothelioma in the age of "Omics": before and after The Cancer Genome Atlas. *J Thorac Cardiovasc Surg*. 2020;160:1078–1083.e2.
14. Mangiante L, Alcala N, Sexton-Oates A, et al. Multiomic analysis of malignant pleural mesothelioma identifies molecular axes and specialized tumor profiles driving intertumor heterogeneity. *Nat Genet*. 2023;55:607–618.
15. Meiller C, Montagne F, Hirsch TZ, et al. Multi-site tumor sampling highlights molecular intra-tumor heterogeneity in malignant pleural mesothelioma. *Genome Med*. 2021;13:113.
16. Giotti B, Dolasia K, Zhao W, et al. Single-cell view of tumor microenvironment gradients in pleural mesothelioma. *Cancer Discov*. 2024;14:2262–2278.
17. Jean D, Daubriac J, Le Pimpec-Barthes F, Galateau-Salle F, Jaurand MC. Molecular changes in mesothelioma with an impact on prognosis and treatment. *Arch Pathol Lab Med*. 2012;136:277–293.
18. Tirosh I, Izar B, Prakadan SM, et al. Dissecting the multicellular ecosystem of metastatic melanoma by single-cell RNA-seq. *Science*. 2016;352:189–196.
19. Barbie DA, Tamayo P, Boehm JS, et al. Systematic RNA interference reveals that oncogenic KRAS-driven cancers require TBK1. *Nature*. 2009;462:108–112.
20. Ianevski A, Giri AK, Aittokallio T. Fully-automated and ultra-fast cell-type identification using specific marker combinations from single-cell transcriptomic data. *Nat Commun*. 2022;13:1246.
21. Efremova M, Vento-Tormo M, Teichmann SA, Vento-Tormo R. CellPhoneDB: inferring cell-cell communication from combined expression of multi-subunit ligand-receptor complexes. *Nat Protoc*. 2020;15:1484–1506.
22. Xue W, Yang L, Chen C, Ashrafizadeh M, Tian Y, Sun R. Wnt/β-catenin-driven EMT regulation in human cancers. *Cell Mol Life Sci*. 2024;81:79.
23. McCarty KS Jr, Miller LS, Cox EB, Konrath J, McCarty KS Sr. Estrogen receptor analyses. Correlation of biochemical and immunohistochemical methods using monoclonal antireceptor antibodies. *Arch Pathol Lab Med*. 1985;109:716–721.
24. Blum Y, Jaurand MC, De Reyniès A, Jean D. Unraveling the cellular heterogeneity of malignant pleural mesothelioma through a deconvolution approach. *Mol Cell Oncol*. 2019;6:1610322.
25. Ou WB, Corson JM, Flynn DL, et al. AXL regulates mesothelioma proliferation and invasiveness. *Oncogene*. 2011;30:1643–1652.
26. Engelsen AST, Lotsberg ML, Abou Khouzam R, et al. Dissecting the role of AXL in cancer immune escape and resistance to immune checkpoint inhibition. *Front Immunol*. 2022;13:869676.
27. Macosko EZ, Basu A, Satija R, et al. Highly parallel genome-wide expression profiling of individual cells using nanoliter droplets. *Cell*. 2015;161:1202–1214.
28. Dobin A, Davis CA, Schlesinger F, et al. STAR: ultrafast universal RNA-seq aligner. *Bioinformatics*. 2013;29:15–21.
29. Palla G, Spitzer H, Klein M, et al. Squidpy: a scalable framework for spatial omics analysis. *Nat Methods*. 2022;19:171–178.
30. Satija R, Farrell JA, Gennert D, Schier AF, Regev A. Spatial reconstruction of single-cell gene expression data. *Nat Biotechnol*. 2015;33:495–502.
31. Fan J, Lee HO, Lee S, et al. Linking transcriptional and genetic tumor heterogeneity through allele analysis of single-cell RNA-seq data. *Genome Res*. 2018;28:1217–1227.
32. Patel AP, Tirosh I, Trombetta JJ, et al. Single-cell RNA-seq highlights intratumoral heterogeneity in primary glioblastoma. *Science*. 2014;344:1396–1401.
33. Tirosh I, Venteicher AS, Hebert C, et al. Single-cell RNA-seq supports a developmental hierarchy in human oligodendroglioma. *Nature*. 2016;539:309–313.
34. Raghavan S, Winter PS, Navia AW, et al. Microenvironment drives cell state, plasticity, and drug response in pancreatic cancer. *Cell*. 2021;184:6119–6137.e26.
35. Robinson MD, McCarthy DJ, Smyth GK. edgeR: a Bioconductor package for differential expression analysis of digital gene expression data. *Bioinformatics*. 2009;26:139–140.
36. Chen Y, McCarthy DJ, Ritchie M, Robinson M, Smyth GK. edgeR: differential expression analysis of digital gene expression data. https://bioconductor.statistik.tu-dortmund.de/packages/3.9/bioc/vignettes/edgeR/inst/doc/edgeRUsersGuide.pdf. Accessed July 17, 2024.
37. Hänzelmann S, Castelo R, Guinney J. GSVA: gene set variation analysis for microarray and RNA-Seq data. *BMC Bioinform*. 2013;14:7.